Journal of Non-Crystalline Solids 354 (2008) 4214–4220

Contents lists available at ScienceDirect

Journal of Non-Crystalline Solids

journal homepage: www.elsevier.com/locate/jnoncrysol

On the role of rotating tetrahedra for generating auxetic behavior in NAT and related systems

Joseph N. Grima *, Victor Zammit, Ruben Gatt, Daphne Attard, Christian Caruana, Trevor G. Chircop Bray

Department of Chemistry, University of Malta, Msida MSD 2080, Malta

ARTICLE INFO

Article history:
Available online 20 August 2008

PACS:
60
62
62.20.-x
62.20.dj

Keyword:
Mechanical properties

ABSTRACT

Systems with negative Poisson's ratios (auxetic) exhibit the unexpected feature of expanding laterally when uniaxially stretched and becoming narrower when compressed. Here, we examine the role of the tetrahedra found in the frameworks of the predicted auxetic zeolites natrolite (NAT), thomsonite (THO) and edingtonite (EDI) for generating negative Poisson's ratios in an attempt to relate the auxeticity in the (001) plane to rotations of the tetrahedra in the zeolite framework. The behavior of the tetrahedra is then examined in terms of their 2D projections in the (001) plane and we show that in the extreme scenario, where the three-dimensional tetrahedra in the zeolite framework are perfectly rigid and simply rotate relative to each other, then their 2D projected behavior in the (001) plane becomes equivalent to the idealized two-dimensional 'rotating squares model' with a Poisson's ratio of −1.

1. Introduction

Auxetic materials or structures exhibit the unusual property of expanding laterally when uniaxially stretched, i.e. they have a negative Poisson's ratio [1–3]. Although auxetics are not commonly encountered in everyday applications, it is well known that they can exist, and in recent years various systems have been reported to exhibit negative Poisson's ratio [1–53]. These systems include various naturally occurring zeolites [4–12] and silicates [13–24] which are crystalline materials characterized by highly intricate geometric frameworks made from MO_4 tetrahedra with M being Si in the case of silicates and typically Si and Al in the case of zeolites.

All of the auxetics discovered so far are characterized by having macro-, micro- or nanostructures with very particular geometric features that allow for auxetic behavior when they deform through appropriate deformation mechanisms. In fact, in recent years, various models have been developed in an attempt to explain the occurrence of negative Poisson's ratios. Such models can be extremely useful as they provide a better insight into the mechanisms by which negative Poisson's ratios can be achieved. In particular the auxetic behavior in the (001) plane of the zeolite natrolite (NAT, chemical composition: $Na_2(Al_2Si_3O_{10}) \cdot 2H_2O$, *Fdd2* symmetry [54]), a zeolite which has been recently reported as auxetic following an off-axis analysis [9] of its experimentally measured elastic constants [8] (see Fig. 1), has been qualitatively described in terms of 2D models involving 'semi-rigid quadrilaterals' [12] (which can be regarded as a more elaborate version of the 'rotating squares' model [4–6,25,26]) while the auxetic behavior in the auxetic silicate α-cristobalite [13–24] has been described in terms of a 2D rotating rectangles model [23,27] and also in terms of a 3D concurrent 'rotating–dilating' tetrahedral model [16–20].

Although 2D models that describe the projected behavior of materials in some particular plane are very commonly used to explain the presence of auxetic behavior, especially since the Poisson's ratio is in itself a two-dimensional property, these models can never fully represent all the deformations that are occurring in three-dimensional auxetic structures or materials. For example, it is important to appreciate that systems such as NAT are in reality 3D systems with a framework made from AlO_4 to SiO_4 tetrahedra. Thus, it is important to have an understanding of how the auxeticity relates to deformations and/or re-orientations in these three-dimensional tetrahedra, and also examine how the projected behavior in the (001) plane, which can be described using 2D models based on 'rotating semi-rigid quadrilaterals', relates to the tetrahedra.

In view of all this, in this paper we will attempt to obtain a better picture of the behavior of the tetrahedra in NAT and related systems (in particular thomsonite (THO) and edingtonite (EDI)) by simulating the properties of hypothetical systems having NAT/THO/EDI-type frameworks where the tetrahedra in the frameworks are all of the same size but have different extents of rigidity so as to investigate whether the auxetic nature of NAT/THO/EDI can be explained, at least partially, in terms of rotating tetrahedra.

* Corresponding author.
E-mail address: joseph.grima@um.edu.mt (J.N. Grima).
URL: http://home.um.edu.mt/auxetic (J.N. Grima).

0022-3093/$ - see front matter © 2008 Elsevier B.V. All rights reserved.
doi:10.1016/j.jnoncrysol.2008.06.081

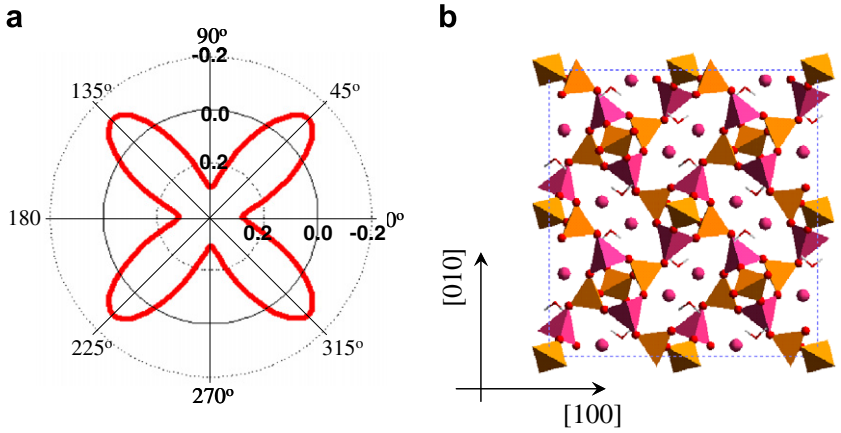

Fig. 1. (a) The Poisson's ratio in the (001) plane as calculated from the experimentally determined elastic constants; and (b) the projection of the NAT framework in the (001) plane. Note that the projection of NAT in this plane is characterized by a 'rotating squares'-type geometry.

2. Method

In this study we performed simulations using the software package Cerius^2 V4.2 (Accelrys Inc.) running on a SGI Octane2 workstation on idealized forms of NAT/THO/EDI-type frameworks where the extent of deformation of the tetrahedra in the frameworks was controlled. In particular, the frameworks used were ones which contained no interstitial species, with all the aluminum atoms in the framework being replaced by silicon atoms (i.e. the SiO_2 equivalents of the empty frameworks). These simplified frameworks were used so simplify the simulations and at the same time accentuate the role of the tetrahedra.

The systems (crystals) were aligned in global *XYZ* space such that the [001] crystal direction is always parallel to the global *Z*-axes and the [010] crystal direction is aligned in the global *YZ*-plane.

Energy expressions for each crystal were set up using modified versions of the Burchart force-field [55] with non-bond terms added using the Ewald summation technique [56] and where the original terms for the Si–O bond stretching and O–Si–O Urey–Bradley were modified from

$$\text{Stretching, Original Burchart}: \quad V_{\text{STR}} = D_{\text{o}}\left(\exp\left[-\sqrt{\frac{k_{\text{s}}}{2D_{\text{o}}}}(l-l_{\text{o}})\right]-1\right)^2 - s. \tag{1}$$

$$\text{Urey–Bradley, Original Burchart}: \quad V_{\text{U–B}} = \frac{1}{2}k_{\text{UB}}(u-u_{\text{o}})^2 + d\cdot k_{\text{UB}}u_{\text{o}}(u-u_{\text{o}}) \tag{2}$$

to

$$\text{Stretching, modified}: \quad V_{\text{STR}} = 10^r\left[\frac{1}{2}k_{\text{s}}(l-l_{\text{o}})^2\right]. \tag{3}$$

$$\text{Urey–Bradley, modified}: \quad V_{\text{UB}} = 10^r\left[\frac{1}{2}k_{\text{UB}}(u-u_{\text{o}})^2\right], \tag{4}$$

where $k_{\text{s}} = 526.0000$ kcal mol^{-1} Å^{-2}, $l_{\text{o}} = 1.5910$ Å, $D_{\text{o}} = s = 350.000$ kcal mol^{-1}, $k_{\text{UB}} = 190.6100$ kcal mol^{-1} Å^{-2}, $u_{\text{o}} = 3.0800$ Å and $d = 0$ (parameters taken from the Burchart force-field [55]). The modified equations permit the control of the extent of rigidity of the tetrahedra through the value of the parameter n which in our simulations was assumed to take values of 0, 0.5, 1 and 2. The resulting 'semi rigid' systems, which we shall henceforth refer to as ZEO_SI_SR(r), ZEO = NAT, THO and EDI, are such that when $r = 0$, the systems will be equivalent to those obtained using the original Burchart force-field (also referred to as ZEO_SI), while the systems with $r = 0.5$, 1 and 2 have tetrahedra which are increasingly more rigid than predicted by the Burchart force-field proper. Note that the other force-field settings, including parameters and terms describing the non-bond interactions and the angles between tetrahedra (i.e. the Si–O–Si Urey–Bradley terms) where left as defined in the force-field, i.e. the 'increased rigidity' of the tetrahedra is relative to these other terms.

Geometry optimisations on $1\times1\times1$ unit cells with periodic boundary conditions were performed to the default Cerius^2 high convergence criteria which include the requirement that the root mean square (RMS) force on each atom must be less than 0.001 kcal mol^{-1} Å^{-1}. No symmetry constraints were used in the minimisations (i.e. the systems were assumed to exhibit a *P1* symmetry). We then simulated the elastic constants from the second derivatives of the energy expressions from which the Poisson's ratios in the (001) plane (i.e. the plane where maximum auxetic behavior was observed) were calculated using standard axis transformation techniques [57]. Note that a $1\times1\times1$ unit cell was used as it was shown that the results obtained were not dependent on the size of unit cell used, i.e. a $1\times1\times1$ unit cell was sufficient for the calculations performed.

We also performed simulations using the modified Burchart force-field where the stiffness constants associated with these two terms where set at the maximum value permitted by Cerius^2 ($k_s = k_{\text{UB}} = 99,999$ kcal mol^{-1} Å^{-1}) so as to estimate the properties of a hypothetical model where the tetrahedra in the SiO_2 equivalents of NAT, THO and EDI are forced to remain as rigid as possible but can easily rotate relative to each other (henceforth referred to as **NAT_SI_R, THO_SI_R** and **EDI_SI_R**, respectively).

Finally, in an attempt to examine the deformations that take place when these systems are mechanically deformed, we also performed simulations where the NAT_SI and NAT_SI_R were uniaxially compressed at 45° to the *x*-axis, (a direction of maximum auxeticity in the case of NAT), where the loads applied were

$$\boldsymbol{\sigma} = \begin{pmatrix} \cos(45^\circ) & \sin(45^\circ) & 0 \\ -\sin(45^\circ) & \cos(45^\circ) & 0 \\ 0 & 0 & 1 \end{pmatrix}\begin{pmatrix} \sigma & 0 & 0 \\ 0 & 0 & 0 \\ 0 & 0 & 0 \end{pmatrix} \times \begin{pmatrix} \cos(45^\circ) & \sin(45^\circ) & 0 \\ -\sin(45^\circ) & \cos(45^\circ) & 0 \\ 0 & 0 & 1 \end{pmatrix}^{\text{T}} = \frac{1}{2}\begin{pmatrix} \sigma & -\sigma & 0 \\ -\sigma & \sigma & 0 \\ 0 & 0 & 0 \end{pmatrix},$$
$$\sigma = -1.00\text{ GPa}, -0.75\text{ GPa}, \ldots, 0.00\text{ GPa} \tag{5}$$

For each minimized system under an applied load, we then measured various lengths and angles corresponding to the quadrilaterals ABCD in the (001) plane (see Fig. 3), and from these we extrapolated the change of these parameters (either as absolute values in the case of angles, or, as percentage changes in the case of lengths) per 0.05E applied stress, where E is the Young's modulus in the direction of loading. A similar analysis was performed on measurements relating to the tetrahedral descriptions of these models, where we measured the properties of the five typical tetrahedra in the system, in particular the ones illustrated in Fig. 2.

Table 1
A comparison of the unit cell parameters of the different systems with each other and with the experimentally determined values

	NAT			THO			EDI		
	a (Å)	b (Å)	c (Å)	a (Å)	b (Å)	c (Å)	a (Å)	b (Å)	c (Å)
Experimental	18.298	18.650	6.559	13.088	13.052	13.229	9.550	9.665	6.523
$r = 0$	18.621	18.621	6.363	13.187	13.187	12.698	9.321	9.321	6.349
$r = 0.5$	18.554	18.554	6.360	13.149	13.149	12.690	9.296	9.296	6.345
$r = 1$	18.397	18.397	6.342	13.113	13.113	12.683	9.272	9.272	6.342
$r = 2$	18.090	18.090	6.273	13.090	13.090	12.679	9.256	9.256	6.340
Rigid	18.038	18.038	6.260	13.089	13.089	12.682	9.255	9.255	6.341

3. Results

3.1. Geometry of the different frameworks

It was observed that in all cases, the minimisations resulted in frameworks with a shape that is very similar to that observed in the actual zeolites, as expected. In particular, as illustrated in Table 1, it was observed that for the same zeolite type, there were only very minimal changes in the cell parameters between the different hypothetical forms modeled. (There were slight decreases in the sizes of the unit cell as the constants describing the rigidity of the tetrahedra increased in the case of NAT, and almost minimal changes in the cases of THO and EDI.)

It was also observed that as these constants increase, the tetrahedra in NAT assumed more regular forms (see Table 2), as expected, with geometric parameters tending to the values defined in the force-fields. Similar trends were also observed in the case of THO and EDI.

Furthermore, when the minimized hypothetical SiO_2 systems equivalent to NAT where examined in terms of the quadrilaterals

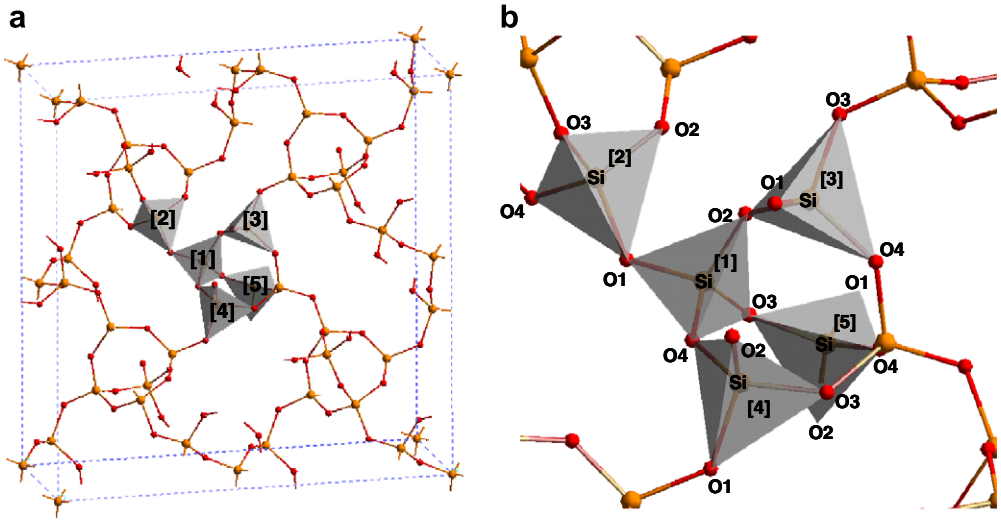

Fig. 2. The arrangement of the five tetrahedra $N = 1,2,...5$ within the NAT framework that are monitored in this study (see Tables 2 and 5).

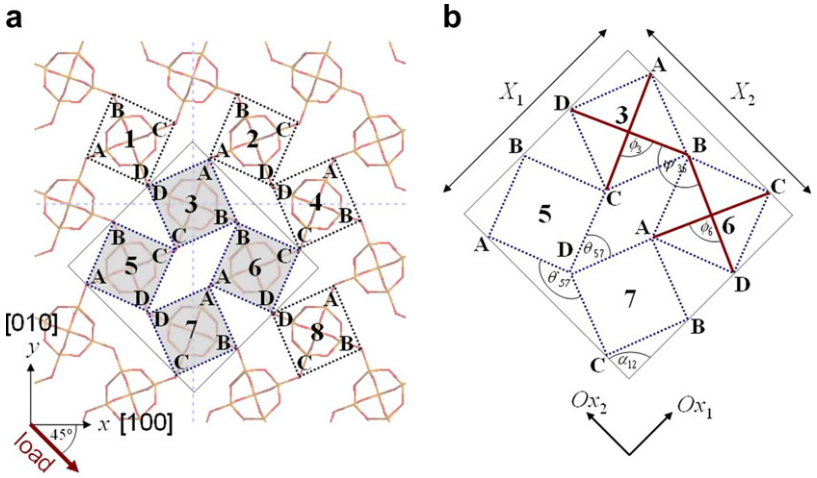

Fig. 3. (a) A 2D projection of the (001) plane of the NAT framework with the eight quadrilaterals $A_nB_nC_nD_n$ (n = 1,...,8) highlighted by dashed lines, and (b) a diagram defining the parameters relating to the quadrilaterals $ABCD$ monitored in this study.

Table 2
Values of geometric parameters associated with typical tetrahedra in the systems for the experimentally determined form of NAT (NAT_EXP), NAT_SI and NAT_SI_R

	$N = 1$	$N = 2$	$N = 3$	$N = 4$	$N = 5$
NAT_EXP					
O1–Si (Å)	1.629	1.738	1.733	1.738	1.615
O2–Si (Å)	1.614	1.736	1.743	1.733	1.615
O3–Si (Å)	1.649	1.733	1.738	1.743	1.627
O4–Si (Å)	1.610	1.743	1.736	1.736	1.627
O1–Si–O2 (°)	111.56	112.15	112.26	108.93	113.10
O1–Si–O3 (°)	107.54	108.93	108.93	104.17	108.24
O1–Si–O4 (°)	107.39	104.17	109.73	112.15	108.32
O2–Si–O3 (°)	109.28	109.73	104.17	112.26	108.32
O2–Si–O4 (°)	111.14	109.52	109.52	109.73	108.24
O3–Si–O4 (°)	109.86	112.26	112.15	109.52	110.63
Si[1] –O–Si[N] (°)	–	129.43	135.81	139.35	144.81
NAT_SI					
O1–Si (Å)	1.585	1.585	1.595	1.585	1.593
O2–Si (Å)	1.605	1.605	1.601	1.595	1.593
O3–Si (Å)	1.595	1.595	1.585	1.601	1.593
O4–Si (Å)	1.601	1.601	1.605	1.605	1.593
O1–Si–O2 (°)	110.50	110.50	108.940	109.38	108.80
O1–Si–O3 (°)	109.38	109.38	109.38	111.69	109.81
O1–Si–O4 (°)	111.69	111.69	108.63	110.50	109.81
O2–Si–O3 (°)	108.63	108.63	111.69	108.94	109.81
O2–Si–O4 (°)	107.64	107.64	107.64	108.63	109.81
O3–Si–O4 (°)	108.94	108.94	110.50	107.64	108.80
Si[1] –O–Si[N] (°)	–	147.72	142.22	142.22	146.08
NAT_SI_R					
O1–Si (Å)	1.592	1.592	1.592	1.592	1.592
O2–Si (Å)	1.592	1.592	1.592	1.592	1.592
O3–Si (Å)	1.592	1.592	1.592	1.592	1.592
O4–Si (Å)	1.592	1.592	1.592	1.592	1.592
O1–Si–O2 (°)	109.49	109.49	109.46	109.45	109.46
O1–Si–O3 (°)	109.45	109.45	109.45	109.50	109.48
O1–Si–O4 (°)	109.50	109.50	109.47	109.49	109.48
O2–Si–O3 (°)	109.47	109.47	109.50	109.46	109.48
O2–Si–O4 (°)	109.45	109.45	109.45	109.47	109.48
O3–Si–O4 (°)	109.46	109.46	109.49	109.45	109.46
Si[1] –O–Si[N] (°)	–	145.33	135.69	135.69	139.13

The parameters measured are defined in Fig. 2.

ABCD projected in the (001) planes, we observed that all quadrilaterals assumed the shape of a square (see Table 3). This contrasts with the properties observed experimentally in NAT proper where the quadrilaterals are parallelograms with side lengths 5.03 Å and 5.08 Å and internal angle of 88.81°.

We also observed that there was a slight decrease in the size of the squares accompanied by a decrease in the angles θ between the squares as the tetrahedra were modeled with higher values of the stiffness constants (see Table 3) which can explain the observed decrease in the unit cell parameters (see Table 1). In the case of THO and EDI, all changes were minimal.

3.2. Mechanical properties

The simulated on-axis mechanical properties for the different frameworks are given in Table 4 while the off-axis mechanical properties in the (001) plane are presented in Fig. 4. These results clearly show that:

1. As the tetrahedra of the SiO_2 equivalents of the zeolites are made more rigid, the auxeticity increases with the Poisson's ratios in the (001) plane tending to an isotropic value of -1 for the rotating rigid tetrahedra (see Fig. 4(b)).
2. The increase in the extent of rigidity of the tetrahedra will result in a significant increase of the on-axis Young's moduli in the [001] direction while there is a minor increase in the moduli in the (001) plane (see Fig. 4(c) and Table 4).
3. As the rigidity of the tetrahedra increases, the shear moduli in the (001) plane increase significantly more than the Young's moduli in the (001) plane indicating that the shear stiffness of the systems in the (001) plane may be approaching infinity in the limit that tetrahedra are perfectly rigid.

3.3. Deformations on the application of stresses

Measurements of the atomic level deformations for NAT_SI and NAT_SI_R are listed in Tables 5 and 6 (which should be compared to the initial values of the respective parameters in Tables 2 and 3). These results clearly suggest that:

1. In NAT_SI_R (but not in NAT_SI), the '3D tetrahedra' and the '2D squares *ABCD*' do not change shape when subjected to stresses.
2. Both systems are such that there are significant changes in the angles between some, but not all, of the tetrahedra.
3. In both systems the deformations have the net effect which can be described in terms of relative rotation of the quadrilaterals *ABCD*s projected in the (001) plane.
4. Any angle changes between different tetrahedra/different squares are more pronounced in NAT_SI_R than in NAT_SI.

4. Discussion

The simulations on the frameworks reported here represent the first attempt at understanding the predicted and/or experimentally measured auxetic character of THO, NAT and EDI in the (001)

Table 3
A description of the 2D projection of NAT in the (001) plane in terms of the 'rotating quadrilaterals' model. The parameters measured are defined in Fig. 3

Data relating to individual quadrilaterals												Angles between two quadrilaterals (degrees)			
Lengths (in Å)							Angles (in degrees)								
n	A_nB_n	B_nC_n	C_nD_n	D_nA_n	A_nC_n	B_nD_n	$A_nB_nC_n$	$B_nC_nD_n$	$C_nD_nA_n$	$D_nA_nB_n$	φ_n	mn	θ_{mn}	θ'_{mn}	ψ_{mn}
NAT EXP															
1, 2, 5, 6	5.08	5.03	5.08	5.03	7.07	7.22	88.81	91.19	88.81	91.19	89.44	Grp I	42.11	137.89	132.12
3, 4, 7, 8	5.08	5.03	5.08	5.03	7.22	7.07	91.19	88.81	91.19	88.81	89.44	Grp II	42.11	137.89	132.12
r = 0 (NAT_SI)															
1, 2, 5, 6	4.86	4.86	4.86	4.86	6.88	6.88	90.00	90.00	90.00	90.00	90.00	Grp I	56.35	123.65	146.35
3, 4, 7, 8	4.86	4.86	4.86	4.86	6.88	6.88	90.00	90.00	90.00	90.00	90.00	Grp II	56.35	123.65	146.35
Rigid															
1, 2, 5, 6	4.79	4.79	4.79	4.79	6.77	6.77	90.00	90.00	90.00	90.00	90.00	Grp I	50.69	129.31	140.69
3, 4, 7, 8	4.79	4.79	4.79	4.79	6.77	6.77	90.00	90.00	90.00	90.00	90.00	Grp II	50.69	129.31	140.69

(Grp I: [mn = 23, 14, 35, 46, 67, 58, 17, 28], Grp II: [mn = 13, 24, 36, 45, 57, 68, 27, 18]).

Table 4
The on-axis mechanical properties for the various SiO_2 systems modeled

(r)	ν_{xy}	ν_{yx}	ν_{xz}	ν_{zx}	ν_{yz}	ν_{zy}	E_x (GPa)	E_y (GPa)	E_z (GPa)	G_{yz} (GPa)	G_{xz} (GPa)	G_{xy} (GPa)
NAT												
0	−0.22	−0.22	0.08	0.37	0.08	0.37	23	23	112	13	13	46
0.5	−0.54	−0.54	0.02	0.18	0.02	0.18	42	42	337	31	31	136
1	−0.80	−0.80	−0.07	−0.74	−0.07	−0.74	53	53	557	63	63	414
2	−0.97	−0.97	−0.01	−0.71	−0.01	−0.71	71	71	3428	138	138	4122
R	−1.00	−1.00	0.00	−0.71	0.00	−0.71	73	73	22 619	152	152	29 593
THO												
0	−0.64	−0.65	0.12	0.41	0.13	0.41	33	33	107	11	12	15
0.5	−0.80	−0.80	0.06	0.34	0.06	0.34	54	55	326	25	25	44
1	−0.91	−0.92	0.02	0.24	0.02	0.24	69	70	1010	38	38	132
2	−0.99	−0.99	−0.01	−0.60	−0.01	−0.60	79	79	9359	49	49	1264
R	−1.00	−1.00	−0.01	−4.27	−0.01	−4.27	80	80	44 605	50	50	9137
EDI												
0	−0.18	−0.18	0.09	0.40	0.09	0.40	24	24	107	12	12	46
0.5	−0.48	−0.48	0.05	0.33	0.05	0.33	46	46	326	25	25	136
1	−0.75	−0.75	0.02	0.24	0.02	0.24	65	65	1009	39	39	402
2	−0.97	−0.97	−0.01	−0.64	−0.01	−0.64	80	80	9292	51	51	3825
R	−1.00	−1.00	−0.01	−4.34	−0.01	−4.34	81	81	43 106	52	52	27 323

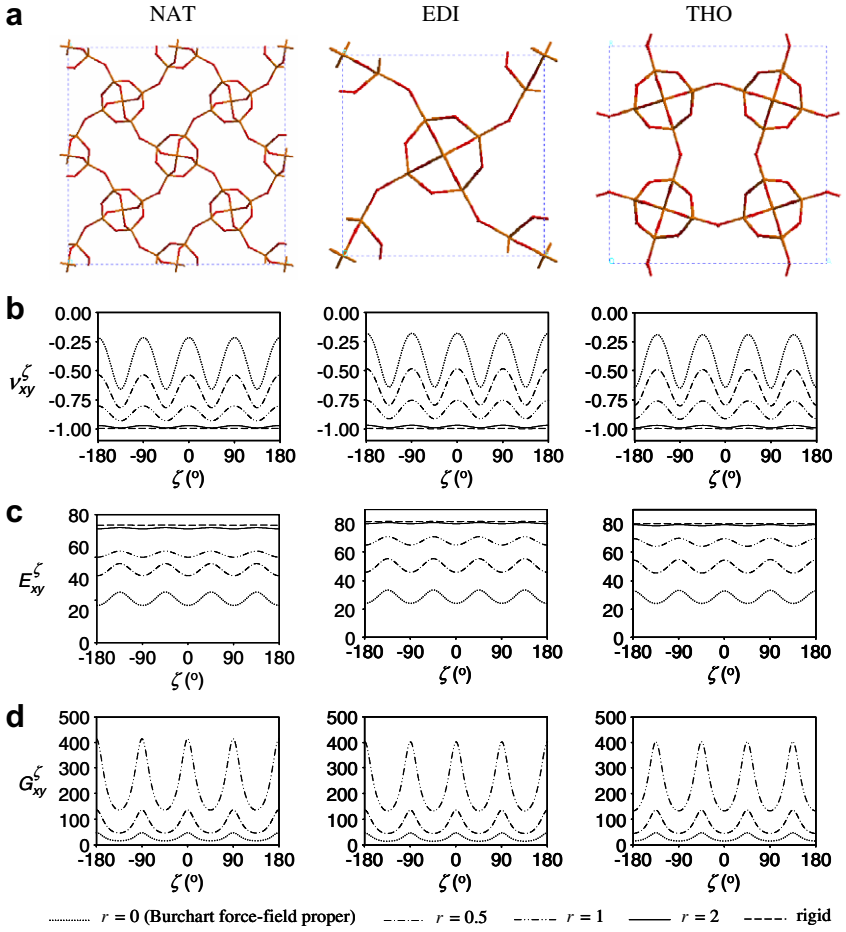

Fig. 4. (a) The structure of NAT, EDI and THO in the (001) plane (shown here are the conformation with the rigid tetrahedral) and the off-axis plots for (b) Poisson's ratios, (c) Young's moduli and (d) shear moduli in the (001) plane for NAT frameworks of different rigidity.

plane, not only in terms of two-dimensional models representing the projected deformations in the (001) plane, but also in terms of the three-dimensional framework of these zeolites. In particular, the approach chosen was one which attempts to assess how the mechanical properties of NAT-type systems change as the tetrahedra in the framework become more rigid, i.e. the frameworks start to approach an idealized 'rotating rigid tetrahedral' model, similar to the one used by Alderson et al. [16–20] to explain the experimentally measured auxeticity in α-cristobalite [13].

An analysis of the values of the elastic constants related to the mechanical properties in the (001) plane of this system clearly suggests that, as the tetrahedra become more rigid, the in-plane Young's moduli and Poisson's ratios behave in such a way that suggests that, in the limit when the tetrahedra are perfectly rigid (i.e.

Table 5
Changes in the geometric parameters associated with tetrahedra (% changes in the case of lengths, actual changes in degrees in the case of angles) per 5% applied strain ($= 0.05 \times E_x^{45}$ GPa, where E_x^{45} is the simulated value of the Young's modulus E_x transformed through axis rotation about z of 45°

	$N = 1$	$N = 2$	$N = 3$	$N = 4$	$N = 5$
NAT_SI					
O1–Si (%)	−0.83	−0.83	0.15	−0.67	−0.03
O2–Si (%)	−0.33	−0.33	0.30	0.15	−0.03
O3–Si (%)	0.25	0.25	−0.67	0.30	−0.15
O4–Si (%)	0.55	0.55	−0.40	−0.40	−0.15
O1–Si–O2 (°)	2.56	2.61	−0.80	−0.96	−0.42
O1–Si–O3 (°)	0.55	0.55	−0.96	−2.00	−0.26
O1–Si–O4 (°)	0.16	0.11	0.21	2.29	−0.23
O2–Si–O3 (°)	−0.86	−0.85	−2.00	−0.80	−0.23
O2–Si–O4 (°)	−0.67	−0.68	1.37	0.21	−0.26
O3–Si–O4 (°)	−1.78	−1.79	2.29	1.37	1.40
Si[1] –O–Si[N] (°)	–	11.38	1.40	1.13	1.29
NAT_SI_R					
O1–Si (%)	−0.03	−0.03	0.00	−0.03	0.00
O2–Si (%)	0.00	0.00	0.00	0.00	0.00
O3–Si (%)	0.00	0.00	−0.03	0.00	0.00
O4–Si (%)	0.00	0.00	0.00	0.00	0.00
O1–Si–O2 (°)	0.02	0.02	−0.01	−0.01	−0.01
O1–Si–O3 (°)	−0.00	−0.00	−0.01	0.00	0.00
O1–Si–O4 (°)	0.01	0.01	0.00	0.02	0.00
O2–Si–O3 (°)	−0.00	−0.00	0.00	−0.01	0.00
O2–Si–O4 (°)	−0.01	−0.01	−0.00	0.00	0.00
O3–Si–O4 (°)	−0.01	−0.01	0.02	−0.00	0.00
Si[1]–O–Si[N] (°)	–	14.46	0.05	0.05	0.05

The parameters measured are defined in Fig. 2.

for an idealized 'rotating rigid tetrahedral' model), they become isotropic in-plane, with Poisson's ratio tending to −1. Furthermore, with increased rigidity of the tetrahedra, the in-plane shear moduli are observed to become much larger than the Young's moduli which only increase to a small extent. All this is very significant as these properties are characteristic of the 2D idealized 'rotating rigid squares' model[1] [25,26] which is commonly used to provide a qualitative explanation for the presence of auxeticity in NAT-type zeolites.

Further evidence linking the simple 2D idealized 'rotating rigid squares' model to the more complex 3D idealized 'rotating rigid tetrahedral' model can be obtained by looking at the measurements listed in Table 6 which clearly shows that in the case of NAT_SI_R, the tetrahedra in the framework are projected in the (001) plane as squares which rotate relative to each other without the squares themselves changing shape or size (to a first approximation). In fact, an analysis of the deformation suggests that this system deforms in such a way that when it is stretched at 45° to the x-direction, deformations of the 'squares' are negligible (less that 0.015% per 5% applied strain in the case of the lengths of the sides/diagonals of the squares, and less than 0.005° per 5% applied stress in the case of the internal angles of the squares, or the angles between the diagonals of the same squares) when compared to a sizable change in the angle between different squares (approx. 14.5° per 5% applied strain).

It is also interesting to note that as illustrated in Table 5, there are significant changes in the angles between some, but not all, of the tetrahedra in the systems modeled. In particular, the simulations suggest that there are two types of inter-tetrahedral connections: those which correspond to tetrahedra coming from 'different squares' (e.g. tetrahedra 1 and 2) which are observed to change significantly when the system is subjected to stresses in the (001) plane, and others (e.g. tetrahedra 1, 3, 4, and 5) which correspond to tetrahedra coming from the 'same square' which were observed

[1] The 'rotating rigid squares' model exhibits in-plane isotropic Poisson's ratios (= 1) and Young's moduli and infinite in-plane shear stiffness.

Table 6
The % changes (for lengths) and actual changes (for angles in degrees) vs. applied stress at 45° to the y-direction (in GPa) for NAT_SI and NAT_SI_R

Data relating to individual quadrilaterals												Changes in angles between two quadrilaterals (degrees)			
% Change in lengths						Changes in angles (angles in degrees)									
n	A_nB_n	B_nC_n	C_nD_n	D_nA_n	A_nC_n	B_nD_n	$A_nB_nC_n$	$B_nC_nD_n$	$C_nD_nA_n$	$D_nA_nB_n$	φ_n	mn	θ_{mn}	θ'_{mn}	ψ_{mn}
r = 0 (NAT_SI)															
1,2,5,6	−0.14	0.73	−0.14	0.73	−0.38	0.97	−0.77	0.77	−0.77	0.77	0.50	Grp I	13.33	−14.87	13.57
3,4,7,8	0.79	−0.21	0.79	−0.21	−0.38	0.96	−0.77	0.77	−0.77	0.77	−0.57	Grp II	14.87	−13.33	14.64
Rigid															
1,2,5,6	0.00	0.01	0.00	0.01	0.00	0.01	0.00	0.00	0.00	0.00	0.00	Grp I	14.50	−14.50	14.50
3,4,7,8	0.01	0.00	0.01	0.00	0.00	0.01	0.00	0.00	0.00	0.00	0.00	Grp II	14.50	−14.50	14.50

These values represent the change (percentage or actual) in the various lengths of sides/diagonals of squares, etc. per 5% applied strain ($= 0.05 \times E_y^{45}$ GPa), where E_y^{45} is the simulated value of the Young's modulus E_x transformed through axis rotation about z of 45°. The parameters monitored are defined in Fig. 3. (Grp I: [mn = 23, 14, 35, 46, 67, 58, 17, 28], Grp II: [mn = 13, 24, 36, 45, 57, 68, 27, 18]).

to remain constant in the simulations of NAT_SI_R under stress. This lack of flexibility in the Si–O–Si angles associated with tetrahedra coming from the 'same square' stems from the way that such tetrahedra are connected together in a cage-like unit which gives these units their characteristic stiffness and make them appear as 'rigid squares' when they are projected in the (001) plane.

All this is very significant as it suggests that the atomic level deformations of an idealized NAT framework projected in the (001) plane approaches the 'idealized rotating squares' model as the tetrahedral units become more rigid, and in the limit when tetrahedra of equal size become fully rigid, the 2D projection of the framework in the (001) plane behaves exactly like the 'idealized rotating squares' model, thus highlighting the relationship between the two modeling approaches (i.e. the approach typically adopted by Alderson et al. [16–20] where 3D frameworks are analyzed in terms of rotating tetrahedra and the alternative approach where the 2D framework is modeled in terms of its 2D projections).

Before we conclude this discussion, it is interesting to note that the simulations reported here also suggest that NAT-type frameworks are predicted to become auxetic in the (100) and (010) planes for loading on-axis if the tetrahedra were to become more rigid, even if these planes are not characterized by the 'rotating squares' geometry found in the (001) plane. Furthermore, it is important to highlight that the behavior in these planes is also characterized by another interesting property, namely that the Young's modulus for loading in the [001] direction becomes much larger than the moduli in the (001) plane which seems to suggests that in the limit that the tetrahedra are perfectly rigid (i.e. for an idealized 'rotating rigid tetrahedral' model), this Young's modulus may tend to infinity.

5. Conclusion

In this work, we investigated the properties of NAT/THO and EDI-type frameworks constructed from tetrahedra having different extents of rigidity. We showed that the mechanical behavior of these frameworks in the (001) plane would tend to the idealized 'rotating rigid squares' if the tetrahedral units in the framework were to be made more rigid, and in the limit that tetrahedra of equal size become fully rigid (i.e. in the idealized 'rotating tetrahedral model'), the 3D 'rotating rigid tetrahedral' model and the 2D 'rotating rigid squares' become equivalent.

This is significant since for the first time, we were able to provide a link between the modeling approach which considers only the 2D projected framework of NAT in the auxetic (001) plane with a more realistic (and more complex) approach involving the tetrahedra present in these systems, thus showing that these two modeling approaches are complimentary and not conflicting with each other.

Acknowledgements

We gratefully acknowledge the support of the Malta Council for Science and Technology (MCST) through their National RTDI funding programme and of the Malta Government Scholarship Scheme (Grant No. ME 367/07/17 awarded to Ms. Daphne Attard).

References

[1] K.E. Evans, M.A. Nkansah, I.J. Hutchinson, S.C. Rogers, Nature 353 (1991) 124.
[2] R.S. Lakes, Science 235 (1987) 1038.
[3] K.W. Wojciechowski, A. Alderson, K.L. Alderson, B. Maruszewski, F. Scarpa, Phys. Stat. Sol. B 244 (2007) 813.
[4] J.N. Grima, A. Alderson, K.E. Evans, Zeolites with negative Poisson's ratios, in: Paper Presented at The RSC 4th International Materials Conference (MC4), Dublin, Ireland, P81, July 1999.
[5] J.N. Grima, R. Jackson, A. Alderson, K.E. Evans, Adv. Mater. 12 (2000) 1912.
[6] J.N. Grima, Ph.D. Thesis, University of Exeter, Exeter, UK, 2000.
[7] J.N. Grima, A. Alderson, K.E. Evans, Phys. Stat. Sol. B 242 (2005) 561.
[8] C. Sanchez-Valle, S.V. Sinogeikin, Z.A.D. Lethbridge, R.I. Walton, C.W. Smith, K.E. Evans, J.D. Bass, J. Appl. Phys. 98 (2005) 053508.
[9] J.N. Grima, R. Gatt, V. Zammit, J.J. Williams, K.E. Evans, A. Alderson, R.I. Walton, J. Appl. Phys. 101 (2007) 086102.
[10] J.N. Grima, V. Zammit, R. Gatt, A. Alderson, K.E. Evans, Phys. Stat. Sol. B 244 (2007) 866.
[11] J.J. Williams, C.W. Smith, K.E. Evans, Z.A.D. Lethbridge, R.I. Walton, Chem. Mater. 19 (2007) 2423.
[12] R. Gatt, V. Zammit, C. Caruana, J.N. Grima, Phys. Stat. Sol. B 245 (2008) 502.
[13] A. Yeganeh-Haeri, D.J. Weidner, D.J. Parise, Science 257 (1992) 650.
[14] N.R. Keskar, J.R. Chelikowsky, Phys. Rev. B 46 (1992) 1.
[15] H. Kimizuka, H. Kaburaki, Y. Kogure, Phys. Rev. Lett. 84 (2000) 5548.
[16] A. Alderson, K.E. Evans, Phys. Chem. Minerals 28 (2001) 711.
[17] A. Alderson, K.E. Evans, Phys. Rev. Lett. 89 (2002) 225503.
[18] A. Alderson, K.L. Alderson, K.E. Evans, J.N. Grima, M. Williams, J. Met. Nano. Mater. 23 (2004) 55.
[19] A. Alderson, K.L. Alderson, K.E. Evans, J.N. Grima, M.R. Williams, P.J. Davies, Comput. Meth. Sci. Technol. 10 (2004) 117.
[20] A. Alderson, K.L. Alderson, K.E. Evans, J.N. Grima, M. Williams, P.J. Davies, Phys. Stat. Sol. B 242 (2005) 499.
[21] H. Kimizuka, H. Kaburaki, Y. Kogure, Phys. Rev. B 67 (2003) 024105.
[22] J.N. Grima, R. Gatt, A. Alderson, K.E. Evans, J. Mater. Chem. 15 (2005) 4003.
[23] J.N. Grima, R. Gatt, A. Alderson, K.E. Evans, Mater. Sci. Eng. A 423 (2006) 219.
[24] H. Kimizuka, S. Ogata, Y. Shibutani, Phys. Stat. Sol. B 244 (2007) 900.
[25] J.N. Grima, K.E. Evans, J. Mater. Sci. Lett. 19 (2000) 1563.
[26] Y. Ishibashi, M.J. Iwata, J. Phys. Soc. Jpn. 69 (2000) 2702.
[27] J.N. Grima, R. Gatt, A. Alderson, K.E. Evans, J. Phys. Soc. Jpn. 74 (2005) 2866.
[28] L.J. Gibson, M.F. Ashby, G.S. Schajer, C.I. Robertson, Proc. Roy. Soc. Lond. A 382 (1982) 25.
[29] R.F. Almgren, J. Elast. 15 (1985) 427.
[30] D. Prall, R.S. Lakes, Int. J. Mech. Sci. 39 (1997) 305.
[31] A. Spadoni, M. Ruzzene, F. Scarpa, Phys. Stat. Sol. B 242 (2005) 695.
[32] K.W. Wojciechowski, Mol. Phys. 61 (1987) 1247.
[33] K.W. Wojciechowski, A.C. Branka, Phys. Rev. A 40 (1989) 7222.
[34] K.W. Wojciechowski, J. Phys. A: Math. Gen. 36 (2003) 11765.
[35] K.E. Evans, M.A. Nkansah, I.J. Hutchinson, Acta Metall. Mater. 2 (1994) 1289.
[36] J.B. Choi, R.S. Lakes, J. Compos. Mater. 29 (1995) 113.
[37] N. Chan, K.E. Evans, J. Cellular Plast. 34 (1998) 231.
[38] C.W. Smith, J.N. Grima, K.E. Evans, Acta Mater. 48 (2000) 4349.
[39] J.N. Grima, A. Alderson, K.E. Evans, J. Phys. Soc. Jpn. 74 (2005) 1341–1342.
[40] K.E. Evans, B.D. Caddock, J. Phys. D: Appl. Phys. 22 (1989) 1883.
[41] A. Alderson, K.E. Evans, J. Mater. Sci. 30 (1995) 3319.
[42] A. Alderson, K.E. Evans, J. Mater. Sci. 32 (1997) 2797.
[43] R.H. Baughman, D.S. Galvao, Nature 365 (1993) 635.
[44] C.B. He, P.W. Liu, A.C. Griffin, Macromolecules 31 (1998) 3145.
[45] J.N. Grima, K.E. Evans, Chem. Commun. (2000) 1531.
[46] J.N. Grima, J.J. Williams, K.E. Evans, Chem. Commun. (32) (2005) 4065.
[47] G.Y. Wei, Phys. Stat. Sol. B 242 (2005) 742.
[48] R.H. Baughman, J.M. Shacklette, A.A. Zakhidov, S. Stafstrom, Nature 392 (1998) 362.
[49] K.V. Tretiakov, K. Wojciechowski, Phys. Stat. Sol. B 244 (2007) 1038.
[50] J.N. Grima, K.E. Evans, J. Mater. Sci. 4 (2006) 3193.
[51] F. Scarpa, F.C. Smith, J. Intel. Mater. Syst. Struct. 15 (2004) 973.
[52] F. Scarpa, W.A. Bullough, P. Lumley, P.I. Mech. Eng. C—J. Mech. Eng. Sci, P.I. Mech. Eng. C-J. Mech. Eng. Sci. 218 (2004) 241.
[53] K.W. Wojciechowski, J. Phys. Soc. Jpn. 72 (2003) 1819.
[54] W.M. Meier, Z. Kristallogr. 113 (1960) 430.
[55] E. de Vos Burchart, Ph.D. Thesis, Technische Universiteit Delft, 1992.
[56] P.P. Ewald, Ann. Phys. 64 (1921) 253.
[57] F. Nye, Physical Properties of Crystals, Clarendon Press, Oxford, 1957.